Some consequences of experiments with a plasmonic quantum eraser for plasmon tomography

L. Grave de Peralta,[1,5,a)] R. Lopez-Boada,[2] A. Ruiz-Columbié,[3] S. Park,[1] and A. A. Bernussi[4,5]
[1]*Department of Physics, Texas Tech University, Lubbock, Texas 79409, USA*
[2]*Department of Natural Science, Health and Wellness, Wolfson Campus, Miami Dade College, Miami, Florida 33132, USA*
[3]*University College, Texas Tech University, Lubbock, Texas 79409, USA*
[4]*Department of Electrical and Computer Engineering, Texas Tech University, Lubbock, Texas 79409, USA*
[5]*Nano Tech Center, Texas Tech University, Lubbock, Texas 79409, USA*

(Received 16 October 2010; accepted 1 December 2010; published online 18 January 2011)

We discuss two important consequences of recent experiments using surface plasmon polariton (SPP) tomography in a quantum eraser arrangement. In these experiments surface-emission images were modified by manipulating the polarization state of the leakage radiation. We show that SPP tomography does have the potential to produce images that mirror with high fidelity the propagation and interference of SPP beams at the metal–air interface of a sample. We reveal the physical mechanism behind this capability of SPP tomography. In addition, we show how SPP tomography can be used to detect photons passing through the dark fringes of an interference pattern and why photons propagate in such a way that looks like a photon can propagate across a region where it is never observed. © *2011 American Institute of Physics*. [doi:10.1063/1.3533730]

I. INTRODUCTION

A plasmonic[1,2] implementation of a quantum eraser[3–6] for imaging applications was recently demonstrated.[7] Using a plasmonic quantum eraser, the authors studied the interference between two perpendicular surface plasmon polariton (SPP) beams excited in a glass-metal sample. They showed that, in order to obtain images that reproduce with high fidelity the interference features formed at the metal–air interface of the sample due to the superposition of the SPP beams, the polarization state of the light leaked through the sample substrate must be controlled.[7]

In this work, we discuss further implications of the experiments reported in Ref. 7 for plasmon tomography applications.[8] Leakage radiation (LR) (Refs. 9–11) and wide-field leakage of plasmon-coupled fluorescence[8] are recently developed SPP-based microscopy techniques which provide high-resolution and raster-free two-dimensional (2D) images. In these microscopy techniques, the images are formed as a result of the collection of light leaked through the substrate of the sample using a high numerical aperture microscope objective lens. Recently, the similitude among microscopy techniques based on the collection of SPP-coupled LR and other tomography imaging techniques has been pointed out.[8] In typical tomography methods,[12] three-dimensional (3D) images are obtained by superposition of numerous 2D images. This is not a requirement in SPP tomography since the SPP propagation occurs confined in a sub-wavelength thick layer containing a metal–dielectric interface.[1,2] In addition, in typical tomography methods, each 2D tomography image is constructed by intensive numerical computation involving numerous one-dimensional (1D) projections. Each 1D projection is obtained by illuminating the object in a different direction.[12] In contrast to conventional tomography methods, in SPP tomography each 1D projection corresponds to the trace in the Fourier-plane image of SPPs propagating in a particular direction.[8] No intensive numerical computation is needed in SPP tomography. Both Fourier-plane and surface-emission images are formed by the arrangement of lenses in the microscope.[8] Throughout this work, we will use the term "SPP tomography" to emphasize that in microscopes based on the collection of SPP-coupled LR, similar to other tomography techniques, the final 2D surface-emission image can be modified by manipulating the "1D projections" in the Fourier plane.[7,9]

In SPP tomography, the photons used for imaging are the ones that, regardless of the measurement process, leak to the sample substrate. This is in contrast to near-field scanning optical microscopy techniques,[13–15] where an optical tip is often placed in close proximity to the region to be imaged. This proximity introduces inevitable perturbations in the original distribution of electromagnetic fields in the sample. The unique nondisturbing capability of SPP tomography techniques makes them specially suited for nondisturbing observation of SPP propagation along the metal–air interface of a sample. However, the question whether the LR profile mirror or not the intensity profile of SPP has been raised in a recent report.[16] Different answers to this key question have been proposed.[11,16] Sometimes, without much consideration about the generality of the assertion, it has been stated that "the direct mapping of the SPP intensity with this method (LR) provides a one-to-one correspondence between the 2D SPP intensity and the image recorded on the charge coupled device (CCD) camera.[11]" Recently, a detailed work[16] concluded that the observed image is proportional to the in-plane intensity distribution of SPPs instead of the intensity of SPPs

a)Electronic mail: luis.grave-de-peralta@ttu.edu.

at the metal–air interface. In that work it has been pointed out that the physical mechanism underlying this phenomenon warrants further investigation. In this work, based on the experimental data obtained using a plasmonic quantum eraser,[7] we address the above question. We show that SPP tomography does have the potential to produce images where the LR profile mirrors the intensity profile of SPPs. We show that the properties of the light that leaks through the glass substrate of the sample can be predicted using a superposition principle which states: (1) light leaks from every point at the sample surface that a SPP excitation passes through, (2) from a given point at the sample surface, light leaks to the sample substrate in the direction of propagation of each SPP excitation passing through that point, and (3) the magnitude of the electric field of the light that leaks from a given point in a given direction is proportional to the magnitude of the electric field of the SPP excitation passing through that point in that direction. We point out here that this superposition principle combined with the dependence of the polarization state of the LR on the direction of propagation of the SPP excitation[17] is the underlying physical mechanism that explain the relation between the observed brightness contrast in the surface-emission image formed by SPP tomography and the SPP intensity distribution existing at the metal–air interface of the sample in observation.

In addition to the implications for imaging methods based on plasmon tomography, the experiments with a plasmonic quantum eraser discussed in this work are also relevant for a deeper understanding of the nature of light. We show that SPP tomography permits to detect photons passing through the dark fringes of an interference pattern. We argue that this is possible because the darkness of the dark fringes observed in an interference pattern does not imply that that the electromagnetic energy density is zero in these regions. Moreover, we present a comprehensive explanation of why it looks like "photons can propagate across a region where they are never observed" in SPP interference experiments recently reported.[18]

II. SPP TOMOGRAPHY ARRANGEMENT AND RESULTS OF CONDUCTED EXPERIMENTS

Figure 1 shows the schematic of the SPP tomography arrangement used in the experiments discussed in this work.[7,18] The excitation source was provided by a 10 mW He–Ne laser (λ=632.8 nm). The laser beam was equally divided by a cube beam splitter (see Fig. 1). Then, the beams were deflected by mirrors toward a low numerical aperture (NA=0.65,40×) microscope objective lens with slightly different angles. As shown in Fig. 2, the lens focused the beams into spots of ~5 μm in diameter at the surface of the sample. Figure 2 shows the schematic of the transversal section of the samples used in the experiments.[7,18] Samples were fabricated on a glass substrate. A 50 nm thick gold layer was initially deposited on top of a 1 nm thick chromium adhesion layer. The gold layer was covered with polymethylmethacrylate (PMMA) as the resist for the e-beam patterning. As sketched in Fig. 2, a pattern containing several scattering features was defined onto the PMMA layer by

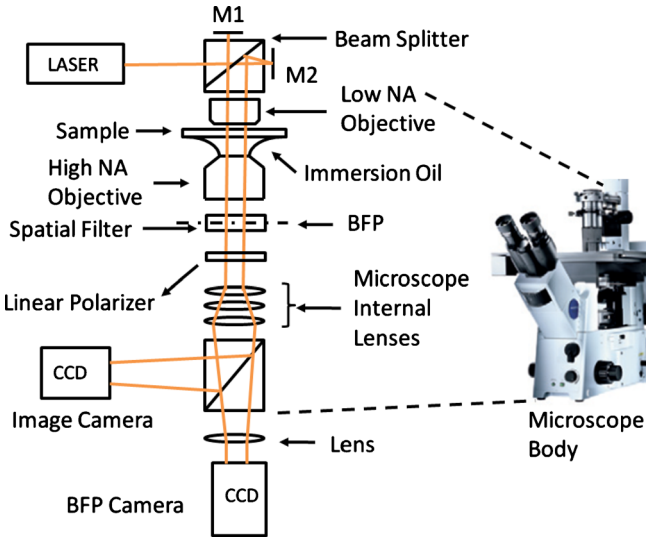

FIG. 1. (Color online) Schematic of the SPP tomography arrangement used in the experiments discussed in this work. M1 and M2 are adjustable mirrors.

e-beam lithography. After developing the PMMA, a second 50 nm thick layer of gold was deposited on the top of the PMMA layer. A final liftoff step produced the desired pattern. Details of the fabricated pattern were published elsewhere.[7,18] Excited SPP propagates along the metal–air interface of the sample, and the radiation that leaked to the substrate was collected by a 100× immersion oil objective lens (NA=1.3). A set of three lenses, internal to the microscope body, perform magnification and aberration correction along with image formation. A CCD camera captures the image of the sample surface emission after being partially reflected by a beam splitter. An external lens and a second CCD camera collect the image formed in the back focal plane (BFP) of the objective. The BFP image corresponds to the Fourier plane with respect to the sample surface emission and thus to a map of the 2D momentum distribution of the LR in the plane of the sample.[7,18] As sketched in Fig. 1, several accessories (spatial filters and a linear polarizer) can

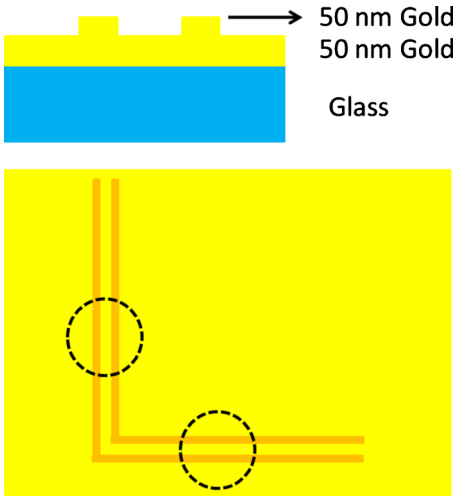

FIG. 2. (Color online) Schematic of (a) transversal section of fabricated samples and (b) scattering features patterned on the sample surface. Dashed circles illustrate the position of the focused spots.

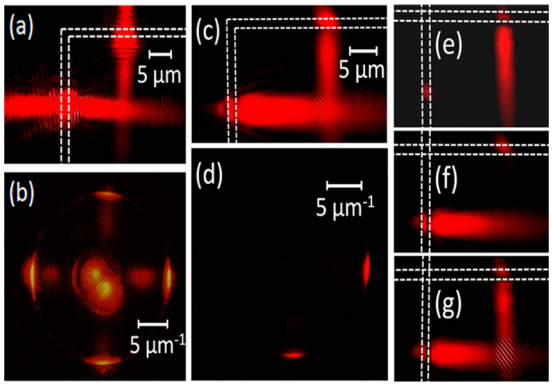

FIG. 3. (Color online) (a) Surface-emission and (b) BFP images obtained by SPP tomography with no accessories introduced after the high NA objective lens. (c) Surface-emission and (d) BFP images obtained after introduction of a spatial filter in the BFP. [(e)–(g)] Surface-emission images obtained with a linear polarizer introduced after the BFP. The direction of the polarizer transmission axis respect to the polarization direction of the SPP-coupled radiation leaked along the SPP beam seen vertical in the images was (e) 0°, (f) 90°, and (g) 45°. The added discontinuous white lines correspond to scattering feature in Fig. 2.

be optionally inserted after the high numerical aperture objective lens. This provides a great deal of flexibility to the SPP tomography arrangement.

Figure 3 shows the surface-emission [Figs. 3(a), 3(c), 3(e), and 3(f)] and BFP [Figs. 3(b) and 3(d)] images obtained by SPP tomography in experiments were a plasmonic quantum eraser was implemented.[7,18] As seen in the surface-emission image shown in Fig. 3(a), four collimated SPP beams were excited by placing a focused spot in each side of a ⌞-shape scattering structure patterned on the surface of the sample (see Fig. 2). Figure 3(b) shows the BFP image corresponding to the surface-emission image shown in Fig. 3(a). The two bright central spots correspond to the fraction of the direct light of the two incident laser spots that traverse the thin gold layer without scattering. The four traces at the right, left, bottom and top extreme in Fig. 3(b) indicate the directions of propagation of the four excited SPP beams. SPP tomography permits to modify the final 2D surface-emission image by manipulating, at the BFP of the microscope, the traces corresponding to particular directions of propagation of SPP along the metal–air interface of the sample. Thus, in order to eliminate the excitation spots and two of the SPP beams shown in Fig. 3(a), an adequate spatial filter was introduced at the BFP (see Fig. 1). As a result, the BFP image shown in Fig. 3(b) was reduced to the BFP image shown in Fig. 3(d). The corresponding surface emission image is shown in Fig. 3(c). The SPP beam launched by the spot focused on the vertical arm of the ⌞ pattern propagates from left to right in Fig. 3(c). This SPP beam produced the bright trace observed in the right extreme of Fig. 3(d). The second SPP beam was launched by the spot focused on the horizontal arm of the ⌞ pattern and propagates from top to bottom in Fig. 3(c). This SPP beam produced the bright trace observed in the bottom extreme of Fig. 3(d).

III. RELATION BETWEEN LR AND SPP PROPAGATION

The surface-emission image shown in Fig. 3(c) is an excellent example of an image formed in a CCD camera of the SPP tomography arrangement shown in Fig. 1 that lacks some important features existing at the metal–air interface of the sample. Only TM polarized SPPs can be excited at the metal–air interface of the sample;[1,2] thus, one should expect to observe clear interference fringes in the region where the two SPP beams cross each other. SPP interference fringes had been observed previously using near-field optical scanning microscopy techniques.[14,15] On the other hand, strong dependence of fringes visibility on the inclination angle of a SPP beam respect to the other has been recently reported using LR techniques.[16] This result raised questions concerning the capability of SPP tomography for providing images that mirror with high fidelity the SPP propagation and interference at the metal–air interface of the sample. However, we have recently demonstrated that using SPP tomography in a quantum eraser arrangement[7,18] permits to obtain surface-emission images [see Fig. 3(g)] that mirror with high fidelity the interference pattern formed at the metal–air interface of the sample. Moreover, it was demonstrated that the absence of clear interference fringes in Fig. 3(c) is due to the different states of polarization of the LR.[7,17] This was confirmed in experiments where a linear polarizer was introduced after the BFP of the high NA objective lens (see Fig. 1). As shown in Figs. 3(e) and 3(f), the insertion of a linear polarizer, with the transmission axis parallel to the polarization direction of the light leaked along the direction of propagation of one of the beams, resulted in the erasure of the another beam from the surface-emission image. As a consequence, when the transmission axis of the linear polarizer was rotated an angle of 45° with respect to the polarization directions of the LR, well-defined interference fringes were observed in the surface-emission image [see Fig. 3(g)].

A careful analysis of the images shown in Fig. 3 permits to reconcile the apparent differences between the results reported in.[7,16] Surface-emission images formed due to the contribution of a single SPP beam [see Figs. 3(e) and 3(f)] indicate that *light leaks from every point of the sample surface that a SPP beam passes through*. BFP images [see Fig. 3(b) and 3(d)] indicate that *light leaks to the sample substrate in the direction of propagation of each excited SPP beam*. Particularly interesting is the presence of well-defined interference fringes in the surface emission image shown in Fig. 3(g). The presence of dark fringes in a surface emission image could be explained by two different mechanisms. The first possibility is that the intensity of the radiation that leaks from a point of the metal–air interface to the sample substrate would be proportional to the square of the total electric field magnitude (intensity) of the SPP excitation at that point. If this was the actual LR mechanism, dark fringes in the surface emission image would occur because no light leaks to the sample substrate from the corresponding point at the metal–air interface. As it will be discussed in Sec. IV, this is not the correct LR mechanism. The actual mechanism involves light leaking in two orthogonal directions from every point in the sample surface contained in the interference minima, i.e., *the magnitude of the electric field of the light that leaks from a given point in a given direction is proportional to the magnitude of the electric field of the SPP excitation passing through that point in that direction*. Superpo-

sition of LR at the CCD camera resulted in the dark fringes observed in the surface-emission image shown in Fig. 3(g). The polarization state of any SPP propagating along the metal–air interface of the sample is TM.[1,2] However, as described in detail in Ref. 17, the polarization state of the LR depends on the direction of SPP propagation. The introduction[7] or removal[16] of a linear polarizer after the high numerical aperture objective lens does not alter the polarization state of the SPP beams propagating along the metal–air interface of the sample or the amount and direction of the light that leaks to the sample substrate. However, this does alter the polarization state of the LR that arrives at the CCD camera. As a consequence, the images obtained with a tomography arrangement without a polarizer[16] differ from the images obtained using SPP tomography in a quantum eraser arrangement.[7,18]

IV. HOW TO DETECT PHOTONS PASSING THROUGH THE DARK FRINGES OF AN INTERFERENCE PATTERN

As shown in Fig. 3(g), well-defined fringes were observed in the region where the beams crossed each other when a linear polarizer was appropriately introduced in the optical path of the leaked light. If no light was emitted from the points at the metal–air interface where interference minima are formed, these points would still appear dark in the surface emission image when the polarizer is removed. As shown in Fig. 3(c), this is not the case. The well-defined fringes present in the surface emission image shown in Fig. 3(g) are not present in the image shown in Fig. 3(c) because light leaks from the points on the sample metal–air interface where the interference minima are formed. Light leaks from these points regardless the position of the polarizer. In these experiments individual photons were not detected. However, as Feynman emphasized "light is made of particles.[19]" Moreover, the corpuscular nature of SPP excitation has been demonstrated experimentally.[20] Thus, we can affirm that SPP tomography permits the detection of photons while they are passing through the dark fringes formed at the region of the metal–air interface where SPP beams cross each other. Figure 4 shows a magnified image of the interference fringes shown in Fig. 3(f). This surface-emission image suggests the idea that somehow photons should pass through the dark fringes defined at the metal–air interface of the sample where the SPP interference minima occur. A photon propagation paradox then arises as to how a photon can propagate across a region where it had never been observed.[18] Certainly, if a conventional photodetector were placed where a dark fringe is formed at the metal–air interface, it would not detect photons at that location. In fact, this is how interference fringes have been observed using near-field optical scanning microscopy techniques.[14] Indeed, the presence of the interference pattern at the metal–air interface of the sample could have been independently corroborated using simultaneously SPP tomography and near-field optical scanning microscopy techniques.[11,21] Nevertheless, the absence of interference fringes in the surface-emission image shown in Fig. 3(c) combined with the superposition principle underlying the image formation in plasmon tomography suggest that: (1) light leaks from the regions on the metal–air interface where the interference minima are formed, (2) photons are really passing through the interference minima, and (3) these photons are observable using SPP tomography techniques. We found that a better understanding of how photons propagate through the interference minima can be obtained by exploring in some detail the electromagnetic energy distribution in the interference pattern. Assuming in a first approximation that the losses due to LR are small, we can approximate the propagation along the metal–air interface of the electromagnetic fields corresponding to the two SPP beams by the propagation in the xz-plane of two perpendicular 2D plane waves. Assuming light polarized in the direction of the y-axis, the electric field of the incident waves can be described by the following expressions:

$$E_{1y}(x,t) = E_o \sin(kx - \omega t), \tag{1}$$

$$E_{2y}(z,t) = E_o \sin(kz - \omega t), \tag{2}$$

where:

$$k = \frac{2\pi}{\lambda}, \quad \omega = 2\pi\nu, \quad \lambda\nu = c/n_{eff}. \tag{3}$$

Here, λ and ν are the SPP wavelength and frequency, respectively; c is the speed of the light in vacuum, and n_{eff} is the effective index of refraction of the SPP excitation. As discussed in Appendix A, in the region where the two waves overlap, the total electric field $E_y(x,z,t)$ is given by the following expression:

$$E_y(x,z,t) = 2E_o \cos\left[\frac{k}{2}(x-z)\right]\sin\left[\frac{k}{2}(x+z) - \omega t\right]. \tag{4}$$

Expression (4) describes a wave within the xz-plane and polarized in the y-direction. The antinodes of the electric field in the interference pattern occur in the regions of the xz-plane where:

$$\cos\left[\frac{k}{2}(x-z)\right] = \pm 1, \tag{5}$$

i.e., in the regions where:

$$z = x + n\lambda, \quad n = 0, \pm 1, \pm 2, \ldots . \tag{6}$$

Expression (6) is the equation of a family of lines that form an angle of 45° with the x-axis. As shown in Fig. 4, the antinodes of the electric field are formed along these lines, i.e., along the bright interference fringes shown in Fig. 4. The dark fringes shown in Fig. 4 occur in the regions of the xz-plane where:

$$\cos\left[\frac{k}{2}(x-z)\right] \equiv 0 \tag{7}$$

I.e., in the regions where:

$$z = x + (2n+1)\frac{\lambda}{2}, \quad n = 0, \pm 1, \pm 2, \ldots . \tag{8}$$

Once an expression for the electric field distribution $E_y(x,z,t)$ is known, the Maxwell's equations can be used to obtain the magnetic field distribution $B_T(x,z,t)$ in the inter-

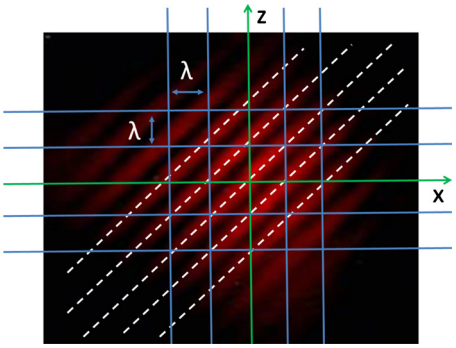

FIG. 4. (Color online) Magnified surface-emission image obtained using SPP tomography in a quantum eraser arrangement corresponding to the interference between two perpendicular SPP beams. Interference maxima are separated by a distance λ in the direction of propagation of the beams. Dashed lines are represented by the equation $z=x\pm n\lambda$.

ference pattern.[22] As discussed in the Appendix B, from expression (4) and the Faraday's induction law follows that:

$$B_T(x,z,t)=2B_o\sin\left[\frac{k}{2}(x-z)\right]\cos\left[\frac{k}{2}(x+z)-\omega t\right]. \quad (9)$$

As shown in the Appendix B, the magnetic field $B_T(x,z,t)$ lies within the xz-plane and oscillates perpendicularly to the direction of the interference fringes shown in Fig. 4. The antinodes of the magnetic field in the interference pattern occur in the regions of the xz-plane where:

$$\sin\left[\frac{k}{2}(x-z)\right]=\pm 1. \quad (10)$$

Thus, the antinodes of $B_T(x,z,t)$ occur in the same regions where the nodes of $E_y(x,z,t)$ are, i.e., in the regions occupied by the dark fringes shown in Fig. 4. The nodes of the magnetic field distribution occur in the regions of the xz-plane where:

$$\sin\left[\frac{k}{2}(x-z)\right]\equiv 0. \quad (11)$$

Thus, the nodes of $B_T(x,z,t)$ occur in the same regions where the antinodes of $E_y(x,z,t)$ are, i.e., in the regions occupied by the bright fringes shown in Fig. 4. These results permit to understand why it appears that photons passing through the dark fringes of the interference pattern are undetectable. The electromagnetic energy carried by light is shared equally by the electric and magnetic fields.[22] Moreover, the electromagnetic energy is basically of electric origin in the bright fringes of the interference pattern but it is of magnetic origin in the dark fringes. The output response of conventional photodetectors is proportional to the temporal average value of the square of the magnitude of the electric field, i.e., proportional to the fraction of the energy carried by the electric field of the electromagnetic wave arriving to the detector.[22,23] Consequently, photons are only detected by conventional photodetectors in the regions occupied by the antinodes of the electric field. The darkness of the dark fringes shown in Fig. 4(g) does not imply that that the electromagnetic energy density is zero in these regions. Photons are not detected in the regions where the dark fringes are formed because in these regions they are associated with the magnetic field. A similar phenomena but for the stationary wave formed when a light beam is reflected by a flat mirror has been studied previously both theoretically and experimentally.[22,23] It is worth studying the electromagnetic field distribution along a line in the direction of propagation of one of the input SPP beams. For instance, the expression describing the electric field along the x-axis at the bright zones of the interference pattern can be obtained using expressions (4) and (6):

$$E_y(x=n\lambda,z=0,t)=\pm 2E_o\sin[n\pi-2\pi\nu t]. \quad (12)$$

Thus,

$$E_y(x=n\lambda,z=0,t=m/\nu)=0,\quad m=0,\pm 1,\pm 2,\ldots. \quad (13)$$

The expression describing the magnetic field along the x-axis at the dark zones of the interference pattern can be obtained using expressions (8) and (9):

$$B_T\left(x=[2n+1]\frac{\lambda}{2},z=0,t\right)=\pm 2B_o\cos\left[(2n+1)\frac{\pi}{2}-2\pi\nu t\right]. \quad (14)$$

Thus,

$$B_T\left(x=[2n+1]\frac{\lambda}{2},z=0,t=m/\nu\right)=\pm 2B_o. \quad (15)$$

As expected from energy conservation considerations, a comparison between expressions (13) and (15) shows that when $E_y=0$ at the antinodes of the electric field distribution in the interference pattern, $|B_T|$ takes is maximum value at the antinodes of the magnetic field distribution. At the times $\tau_m=m/\nu$ the electromagnetic energy is concentrated in the bright fringes of the interference pattern. At times where $\tau'_m=(2m+1)/2\nu$ the electromagnetic energy is concentrated in the dark fringes of the interference pattern. Thus, the electromagnetic energy flows through the interference pattern (in the original direction of the incident SPP beams) alternating from the electric to the magnetic fields and conversely. Photons are detectable using conventional photodetectors when the electromagnetic energy is carried by the electric field in the bright fringes of the interference pattern. However, photons are undetectable using conventional photo-detectors when the electromagnetic energy is carried by the magnetic field. This occurs in the dark fringes of the interference pattern.

V. CONCLUSIONS

In this work, based on experimental data obtained in recent experiment using SPP tomography in a quantum eraser arrangement, we discussed two important consequences for SPP tomography. First, we showed that SPP tomography does have the potential to produce images which mirror with high fidelity the propagation and interference of SPP beams at the metal–air interface of a sample. In order to realize this potential, one has to be able to manipulate the

polarization state of the LR. In addition, we showed that the properties of the light that leaks through the glass substrate of the sample can be predicted using a superposition principle which states: (1) light leaks from every point of the sample surface that a SPP excitation passes through, (2) from a given point at the sample surface, light leaks to the sample substrate in the direction of propagation of each SPP excitation passing through that point, and (3) the magnitude of the electric field of the light that leaks from a given point in a given direction is proportional to the magnitude of the electric field of the SPP excitation passing through that point in that direction. We pointed out that this superposition principle combined with the dependence of the polarization state of the LR on the direction of propagation of the SPP excitation is the underlying physical mechanism that explain the relation between the observed brightness contrast in the surface-emission image formed by SPP tomography and the SPP intensity distribution existing in the metal–air interface of a the sample in observation. Second, we showed how SPP tomography can be used to detect photons passing through the dark fringes of an interference pattern. We calculated the spatial and temporal distribution of the electric and magnetic field at the metal–air interface in the discussed experiments, and the obtained results were used to explain why photons propagate in such a way that looks like a photon can propagate across a region where it is never observed. We argued that this is because the darkness of the dark fringes observed in the interference pattern does not imply that that the electromagnetic energy density is zero in these regions.

ACKNOWLEDGMENTS

This work was partially supported by the NSF CAREER Award (Grant No. ECCS-0954490), U.S. Army CERDEC Contract (Grant No. W15P7T-07-D-P040), and the J. F. Maddox Foundation.

APPENDIX A

Expression (4) can be obtained by adding expressions (1) and (2):

$$E_y(x,z,t) = E_o[\sin(kx-\omega t) + \sin(kz-\omega t)]. \tag{A1}$$

Doing:

$$\alpha = kx-\omega t, \quad \beta = kz-\omega t. \tag{A2}$$

And using the trigonometric identity:

$$\sin\alpha + \sin\beta = 2\cos\left[\frac{1}{2}(\alpha-\beta)\right]\sin\left[\frac{1}{2}(\alpha+\beta)\right]. \tag{A3}$$

APPENDIX B

The Faraday's induction law can be written in terms of the components of the electric and magnetic fields as:[23]

$$\frac{\partial E_z}{\partial y} - \frac{\partial E_y}{\partial z} = -\frac{\partial B_x}{\partial t}, \quad \frac{\partial E_x}{\partial z} - \frac{\partial E_z}{\partial x} = -\frac{\partial B_y}{\partial t}, \quad \frac{\partial E_y}{\partial x} - \frac{\partial E_x}{\partial y} = -\frac{\partial B_z}{\partial t}. \tag{B1}$$

Thus,

$$B_x = \int \frac{\partial E_y}{\partial z}dt, \quad \frac{\partial B_y}{\partial t} \equiv 0, \quad B_z = -\int \frac{\partial E_y}{\partial x}dt. \tag{B2}$$

The z-component of the magnetic field can be expressed as:

$$B_z(x,t) = B_o \sin[kx-\omega t], \tag{B3}$$

where:

$$\frac{kE_o}{\omega} = \frac{2\pi/\lambda}{2\pi\nu}E_o = \frac{E_o}{c} = B_o. \tag{B4}$$

Expression (B3) can be calculated from the derivative of (4) with respect to the variable x, followed by doing:

$$\gamma = \frac{k}{2}(x-z), \quad \delta = \frac{k}{2}(x+z) - \omega t, \tag{B5}$$

using the trigonometric identity:

$$\cos(\gamma+\delta) = \cos\gamma\cos\delta - \sin\gamma\sin\delta, \tag{B6}$$

and using expression (B2). $B_z(x,t)$ corresponds to the magnetic field of a plane wave propagating in the direction of the x-axis with the magnetic field oscillating in the direction of the z-axis. The x-component of the magnetic field:

$$B_x(z,t) = -B_o \sin[kz-\omega t], \tag{B7}$$

can be calculated from the derivative of (4) respect to the variable z, followed by using expression (B5), the trigonometric identity:

$$\cos(\gamma-\delta) = \cos\gamma\cos\delta + \sin\gamma\sin\delta, \tag{B8}$$

and using the expression (B2). $B_x(z,t)$ corresponds to the magnetic field of a plane wave propagating in the direction of the z-axis with the magnetic field oscillating in the direction of the x-axis. From expressions (B3) and (B7) follow that the total magnetic field $B_T(x,z,t)$ oscillates in the plane xz perpendicularly to the interference fringes shown in Fig. 4:

$$B_T(x,z,t) = B_z(x,t) + B_x(z,t) = B_o[\sin(kx-\omega t) - \sin(kz-\omega t)]. \tag{B9}$$

Finally, (B9) can be rewritten as (9) using (A2) and the trigonometric identity:

$$\sin\alpha - \sin\beta = 2\sin\left[\frac{1}{2}(\alpha-\beta)\right]\cos\left[\frac{1}{2}(\alpha+\beta)\right]. \tag{B10}$$

[1] M. H. Raether, *Surface Plasmons on Smooth and Rough Surfaces and on Gratings* (Springer-Verlag, New York, 1988).
[2] D. Sarid and W. Challener, *Modern Introduction to Surface Plasmons: Theory, Mathematica Modeling, and Applications* (Cambridge University Press, New York, 2010).
[3] M. O. Scully and K. Drühl, Phys. Rev. A **25**, 2208 (1982).
[4] T. J. Herzog, P. G. Kwiat, H. Weinfurter, and A. Zeilinger, Phys. Rev. Lett. **75**, 3034 (1995).
[5] S. P. Walborn, M. O. Terra Cunha, S. Pádua, and C. H. Monken, Phys. Rev. A **65**, 033818 (2002).
[6] W. Holladay, Phys. Lett. A **183**, 280 (1993).
[7] J. Ajimo, M. Marchante, A. Krishnan, A. A. Bernussi, and L. Grave de Peralta, J. Appl. Phys. **108**, 063110 (2010).
[8] S. P. Frisbie, C. Chesnutt, M. E. Holtz, A. Krishnan, L. Grave de Peralta, and A. A. Bernussi, IEEE Photonics Journal **1**, 153 (2009).
[9] A. Drezet, A. Hohenau, A. L. Stepanov, H. Ditlbacher, B. Steinberger, N. Galler, F. R. Aussenegg, A. Leitner, and J. R. Krenn, Appl. Phys. Lett. **89**,

091117 (2006).
[10]S. Massenot, J. Grandidier, A. Bouhelier, G. Colas des Francs, L. Markey, J.-C. Weeber, A. Dereux, J. Renger, M. U. Gonzàlez, and R. Quidant, Appl. Phys. Lett. **91**, 243102 (2007).
[11]A. Drezet, A. Hohenau, D. Koller, A. Stepanov, H. Ditlbacher, B. Steinberger, F. R. Aussenegg, A. Leitner, and J. R. Krenn, Mater. Sci. Eng., B **149**, 220 (2008).
[12]A. C. Kak and M. Slaney, *Principles of Computerized Tomographic Imaging* (IEEE, New York, 1988).
[13]D. W. Pohl, W. Denk, and M. Lanz, Appl. Phys. Lett. **44**, 651 (1984).
[14]A. Passian, A. Wig, A. L. Lereu, P. G. Evans, F. Mariaudeau, T. Thundat, and T. L. Ferrell, Ultramicroscopy **100**, 429 (2004).
[15]J.-C. Weeber, J. R. Krenn, A. Dereux, B. Lamprecht, Y. Lacroute, and J. P. Goudonnet, Phys. Rev. B **64**, 045411 (2001).
[16]J. Wang, C. Zhao, and J. Zhang, Opt. Lett. **35**, 1944 (2010).
[17]C. S. P. Frisbie, C. Chesnutt, J. Ajimo, A. A. Bernussi, and L. Grave de Peralta, Opt. Commun. **283**, 5255 (2010).
[18]L. Grave de Peralta, J. Opt. Soc. Am. B **27**, 1513 (2010).
[19]R. P. Feynman, *QED: The Strange Theory of Light and Matter* (Princeton University Press, Princeton, 1985).
[20]E. Altewischer, M. P. van Exter, and J. P. Woerdman, Nature (London) **418**, 304 (2002).
[21]E. B. Steinberger, A. Hohenau, H. Ditlbacher, F. R. Aussenegg, A. Leitner, and J. R. Krenn, Appl. Phys. Lett. **91**, 081111 (2007).
[22]E. Hetcht, *Optics*, 4th ed. (Pearson-Addison Wesley, New York, 2002).
[23]M. Born and E. Wolf, *Principles of Optics*, 5th ed. (Pergamon, Oxford, 1975), pp. 277–281.